Segregation-controlled kinetics of fast impurity diffusion in polycrystalline solids

1996 J. Phys.: Condens. Matter 8 5843

(http://iopscience.iop.org/0953-8984/8/32/005)

J. Phys.: Condens. Matter **8** (1996) 5843–5856. Printed in the UK

Segregation-controlled kinetics of fast impurity diffusion in polycrystalline solids

N A Stolwijk†, Ch Poisson‡ and J Bernardini‡

† Institut für Metallforschung, Universität Münster, Wilhelm-Klemm-Strasse 10, D-48149 Münster, Germany

‡ Laboratoire de Métallurgie, CNRS URA 443, Faculté des Sciences de Saint-Jérôme, Avenue Escadrille Normandie–Niemen, 13397 Marseille Cédex 20, France

Received 17 January 1996, in final form 2 May 1996

Abstract. Commonly, the presence of grain boundaries in crystalline solids leads to enhanced atomic transport because atoms can move faster along such two-dimensional lattice defects than through the lattice itself. Recent experiments on gold diffusion into silicon, however, showed for the first time a retardation of the metallic impurity incorporation in polycrystalline material compared to that of monocrystals of the same host. The present paper provides a new model that accounts for the experimental findings with regard to Si:Au. In addition, it may apply to other systems in which a high mobility of the impurity in the lattice goes along with extremely strong segregation effects.

1. Introduction

In the past few decades grain boundary (GB) diffusion in metals has been the subject of extensive studies [1, 2]. As the most prominent result it is always found that both impurity and self-atoms move faster along GBs than through the grains themselves (ignoring hydrogen as the only established exception). To put this differently, the GB diffusion coefficient D_b is larger than the corresponding lattice diffusivity D. This may not surprise since GBs represent disturbed lattice regions with reduced atomic density providing more space for atomic displacements.

The circumstance that the diffusivity along GBs substantially exceeds that in the adjacent lattice ($D_b \gg D$) gives rise to a distinct temporal evolution of the in-diffusion process in polycrystalline materials (i.e. with stationary grains). Following Harrison ([3]; see also [4]), three major kinetic regimes designated by A, B, C may be distinguished in substrates with grain size G, GB width $\delta \approx 0.5$ nm and segregation coefficient $s = C_b/C$. The latter dimensionless quantity reflects the ratio of the impurity (volume) concentration in GBs (C_b) to that in the adjacent lattice (C) and is usually greater than one. Regimes A, B, C become manifest in the diffusion profile, that is, by monitoring the average concentration $\bar{C}$ in layers parallel to the (impurity-deposited) surface as a function of penetration depth y.

The diffusion process enters Harrison's regime C immediately after the onset of annealing and stays there for times t which are so short that $(Dt)^{1/2} \ll (1/2)s\delta$. As an implication, leakage of the impurity from the boundaries to the lattice is negligible. In other words, atomic transport exclusively proceeds through GBs. For an inexhaustible impurity source the diffusion profile adopts the complementary error function shape while

0953-8984/96/325843+14$19.50

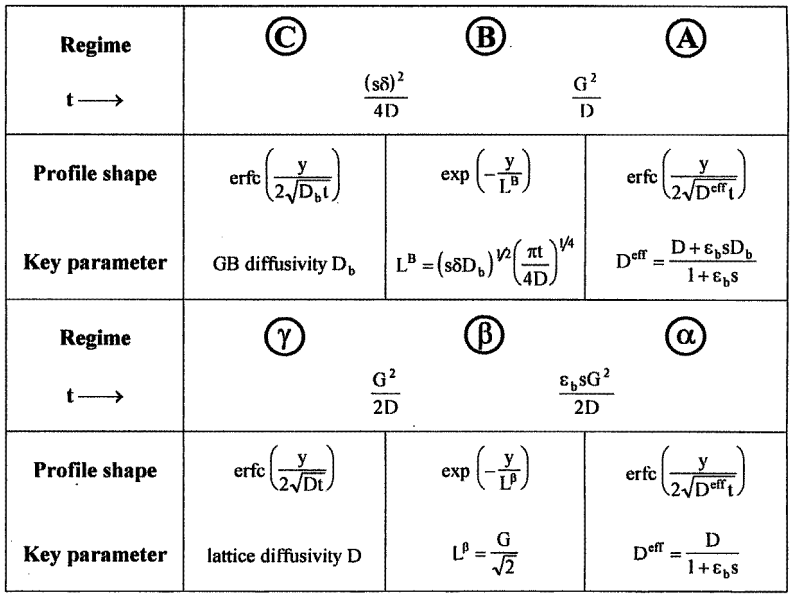

Figure 1. Evolution of the impurity incorporation in polycrystalline materials with diffusion time t. Upper half: kinetic regimes C, B, A for $D_b \gg D$ according to Harrison's classification. Lower half: kinetic regimes γ, β, α for $\varepsilon_b s D_b \ll D$ in conjunction with $\varepsilon_b s \gg 1$ according to the present model. Transition times between different regimes are also indicated. Notation: penetration depth y, grain size G, GB width δ, GB volume fraction ε_b and segregation coefficient s. Additional labelling of D, D^{eff}, L^β and s in the lower half with the subscripts i or is makes this diagram specific for interstitial or interstitial–substitutional impurities (see the text).

the penetration depth $L^C = (D_b t)^{1/2}$ is determined by the GB diffusivity. These features are indicated in figure 1.

Regime B is correlated with intermediate diffusion times restricted to $(1/2)s\delta \ll (Dt)^{1/2} \ll G$. Impurity incorporation in this regime is governed by long-distance penetration along GBs and subsequent out-diffusion from the boundaries into the lattice. According to Fisher's approximation [5] this induces impurity profiles of exponential shape with a characteristic depth scale $L^B = (s\delta D_b)^{1/2}(\pi t/4D)^{1/4}$ depending on both D_b and D (cf. figure 1). In more elaborate treatments of Fisher's model [2, 6] the initially predicted proportionality $\ln \bar{C} \propto y$ is modified to $\ln \bar{C} \propto y^{6/5}$. This slight difference, however, is hardly observable experimentally and not significant in the present context. More important is the notion that within the time limits of regime B, L^B exceeds the lattice diffusion length $(Dt)^{1/2}$.

Regime A establishes for $(Dt)^{1/2} \gg G$, which reflects that individual GBs must no longer be regarded as isolated from each other after sufficiently long diffusion time. Rather we are dealing with a situation in which diffusing impurities encounter several or many GBs. Following Hart's approach [7] (originally proposed for diffusion in dislocated crystals) impurity incorporation is controlled by the effective diffusivity

$$D^{eff} = (1 - \tau)D + \tau D_b \tag{1}$$

where τ and $1 - \tau$ refer to the fractions of time that a diffusing atom spends in GBs and the lattice, respectively. The time fraction τ may be estimated from the relative abundancies

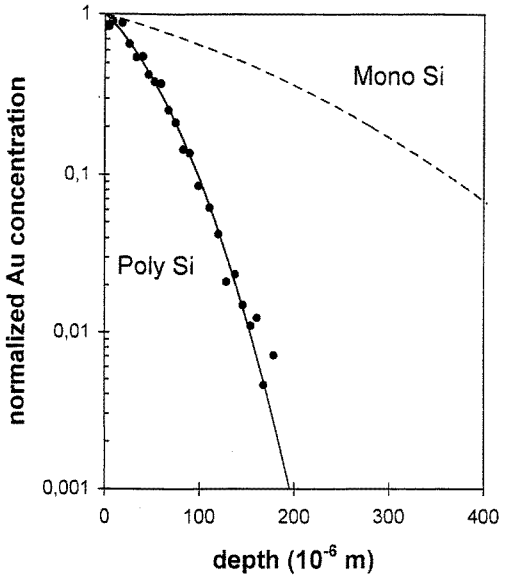

Figure 2. A comparison of Au diffusion in poly- and monocrystalline silicon. Circles and solid-line erfc fit: the ^{195}Au profile measured after 3600 s of diffusion at 1254 K into high-purity polycrystalline Si [8]. Dashed line: the corresponding erfc profile for monocrystalline Si based on an interpolation of experimental data [10, 11]. The differences in concentration levels between the two profiles are arbitrary due to normalization along the ordinate.

of GB and lattice sites as

$$\tau = \frac{\varepsilon_b C_b}{(1-\varepsilon_b)C + \varepsilon_b C_b} \approx \frac{\varepsilon_b s}{1+\varepsilon_b s} \tag{2}$$

where the GB volume fraction $\varepsilon_b \ll 1$ is given by

$$\varepsilon_b = \frac{q\delta}{G}. \tag{3}$$

The numerical factor q equals 3 for cubic grains and is close to 2 for real grain structures [2]. Combining equations (1) and (2) leads to

$$D^{eff} = D\frac{1+\varepsilon_b s D_b/D}{1+\varepsilon_b s}. \tag{4}$$

It is important to note that the common property $D_b > D$ implies that $D^{eff} \geqslant D$. To be specific, the A-regime diffusivity given by equation (4) runs from the lattice diffusivity D in coarse-grained polycrystals ($\varepsilon_b s D_b/D \ll 1$) to the GB diffusivity D_b in extreme cases of ultrafine-grained material ($\varepsilon_b s \gg 1$) [2, 4].

In summary, we emphasize that for $D_b > D$ the overall impurity penetration tends to be larger in polycrystals than in monocrystals of the same host material, irrespective of the kinetic regime considered. Conversely, when experimental data show retarded diffusion in polycrystals compared to corresponding monocrystals, this cannot be reconciled with $D_b > D$ but rather points to the opposite condition. Observations of this kind have recently been made for Au in Si [8, 9] as illustrated by figures 2 and 3. Specifically, it is seen here that the penetration depths in polycrystalline Si are smaller than those corresponding to the diffusion coefficients determined for monocrystalline samples [10, 11]. An extensive account of the experimental findings will be given elsewhere [12]. In the present paper

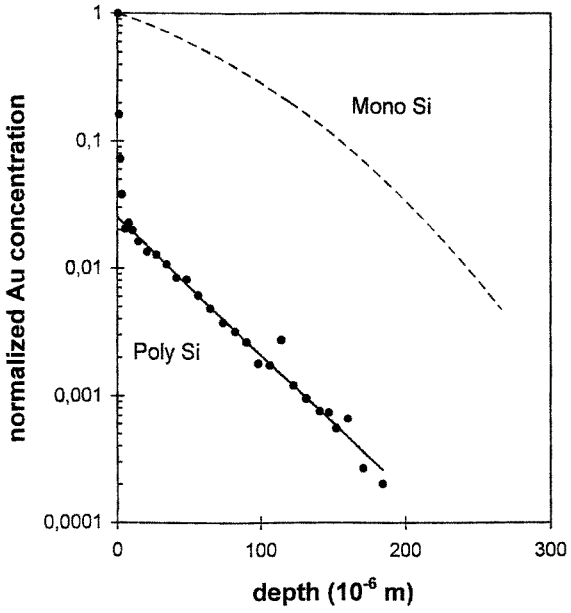

Figure 3. A comparison of Au diffusion in poly- and monocrystalline silicon. Circles and straight-line fit: the ^{195}Au profile measured after 145 440 s of diffusion at 934 K into electronic-grade polycrystalline Si with grain sizes around 30 mm [8]. Dashed line: the corresponding erfc profile for monocrystalline Si based on an extrapolation of experimental data [10, 11]. Differences in concentration levels between the two profiles are arbitrary due to normalization of ordinate values.

we propose a new kinetic model that explains crucial observations on the polycrystalline Si:Au system. In addition, our concepts may be applicable to other impurity–host systems in which fast lattice diffusion is accompanied by strong segregation effects and negligible GB diffusion.

2. The theoretical model

2.1. Basic concepts

We start from the following assumptions applying to an impurity X in an otherwise pure matrix.

(i) The impurity has a high diffusivity D_i in the interstitial configuration X_i.

(ii) The impurity may strongly segregate to grain boundary sites B where it adopts the X_b configuration.

(iii) The interaction between impurities and grain boundaries is described by the quasi-chemical reaction

$$X_i + B \underset{k_{b-}}{\overset{k_{b+}}{\leftrightarrow}} X_b + E \tag{5}$$

where E stands for an empty interstitial site. The reaction rates in the forward and reverse directions are denoted by k_{b+} and k_{b-}, respectively.

(iv) Segregation is supposed to be linear (Henry-type), that is, impurity saturation effects of the grain boundary are ignored.

(v) Impurity diffusion along grain boundaries (GBs) characterized by D_b proceeds much more slowly than through the lattice. As will be discussed in section 3, D_b may be envisaged as the effective diffusivity of segregated impurities comprising mobile as well as immobile atoms.

(vi) Grain boundary sites B are conceived to be randomly distributed over the volume. This forms an adequate picture provided that the overall X-penetration depth y exceeds the mean GB size G and that concentrations are averaged over planes parallel to the (flat) surface ($y = 0$) intersecting many grains. The latter condition complies with the standard radiotracer technique which includes serial sectioning of the diffused sample. Within this framework the distinction between $C_j = C_j(x, y, z, t)$ and $\bar{C}_j = \bar{C}_j(y, t)$ vanishes and the upper bar indicating thin-layer averages will be dropped henceforward.

(vii) Interactions of the impurity with dislocations are considered to be negligible.

Several of these assumptions will be made specific below. In the general formulation given above the evolution of the diffusion–segregation process with time t may be described in one-dimensional geometry by the following equations:

$$\frac{\partial C_b}{\partial t} = D_b \frac{\partial^2 C_b}{\partial y^2} + (1 - \varepsilon_b)(k_{b+} C_i C_{b0} - k_{b-} C_b C_{i0}) \tag{6a}$$

$$\frac{\partial C_i}{\partial t} = D_i \frac{\partial^2 C_i}{\partial y^2} - \varepsilon_b (k_{b+} C_i C_{b0} - k_{b-} C_b C_{i0}). \tag{6b}$$

Here $C_i = C_i(y, t)$ and $C_b = C_b(y, t)$ are volume concentrations of X_i and X_b, respectively. C_{i0} (C_{b0}) refers to the atomic site density of the interstitial lattice (grain boundaries) which is likely to be close to the substitutional lattice site density C_{s0} (e.g. 5.00×10^{28} m^{-3} for Si). We emphasize that C_b is as usual defined with respect to the GB volume (and similarly, C_i to the lattice volume). Directly connected with this, the factor ε_b in equation (6*b*) rescales C_b and C_{b0} to the overall matrix volume. The corresponding factors $1 - \varepsilon_b$ for C_i and C_{i0} cancel against each other on both sides of the equality sign in equation (6*b*). In contrast, in equation (6*a*) ε_b is cancelled and $1 - \varepsilon_b$ survives. In the following we take it for granted that $1 - \varepsilon_b \approx 1$ holds to a very good approximation†.

The equilibrium (or terminal) concentrations of X_i and X_b indicated by C_i^{eq} and C_b^{eq}, respectively, obey the mass action law with regard to equation (5), i.e.,

$$\frac{C_b^{eq} C_{i0}}{C_i^{eq} C_{b0}} = \frac{k_{b+}}{k_{b-}}. \tag{7}$$

C_i^{eq} establishes by exchange with a second phase containing the impurity, e.g. ambient gas or an alloy formed at the surface after deposition of pure X. In turn, C_i^{eq} determines C_b^{eq} through equation (7). The terminal state of the reacting system described by equation (7) must be differentiated from conditions of *local dynamic* equilibrium expressed as

$$\frac{C_b C_{i0}}{C_i C_{b0}} = \frac{k_{b+}}{k_{b-}} \tag{8}$$

which may hold to a very good approximation for sufficiently long diffusion times. Based on equations (5) and (8) we can distinguish between different kinetic regimes in the temporal evolution of the impurity distribution.

(i) Regime α: for long diffusion times local dynamic equilibrium among X_i and X_b is settled almost wholly over the entire X-penetrated zone. It will be shown below that GB

† It should be noted that this approximation leads to symmetry breaking with respect to interchanging the role of X_i and X_b. According to equation (3) $\varepsilon_b < 0.01$ is connected with grain sizes larger than 0.1 μm, which corresponds to common polycrystalline materials.

segregation affects the depth but not the shape of the penetration profile characteristic for lattice diffusion.

(ii) Regime β: for intermediate times segregation already controls the diffusion kinetics but equilibrium among the reacting species according to equation (8) has not established yet. This regime may be recognized from the modified shape of the X distribution with respect to regimes α and γ.

(iii) Regime γ: shortly after the onset of diffusion the segregation effect is still very minor. Incorporation of the impurity mainly takes place in the lattice and is governed by the lattice diffusivity accordingly.

In the following sections we will derive expressions for the impurity distribution in each kinetic regime. All solutions are given for constant boundary concentrations imposed by an inexhaustible foreign-atom source. For the sake of clarity, we will deal with purely interstitial impurities first and then treat the more elaborate case of so-called interstitial–substitutional impurities. The latter case complies with recently obtained experimental data on Au in Si [8, 9, 12].

2.2. Interstitial impurities

2.2.1. Regime α: long diffusion times. From the validity of equation (8) after sufficiently prolonged diffusion one obtains with the aid of equation (7)

$$C_b = \frac{C_b^{eq}}{C_i^{eq}} C_i. \tag{9}$$

Addition of equations (6*a*) and (6*b*) while accounting for the appropriate weighing factors ϵ_b and $1 - \varepsilon_b \approx 1$, respectively, yields the time derivative of the total X concentration C_t:

$$C_t = C_i + \varepsilon_b C_b \tag{10}$$

as

$$\frac{\partial C_t}{\partial t} = D_i \frac{\partial^2 C_i}{\partial y^2} + \varepsilon_b D_b \frac{\partial^2 C_b}{\partial y^2}. \tag{11}$$

Using equation (9), this expression can be cast into the form of Fick's second law, i.e.,

$$\frac{\partial C_i}{\partial t} = \frac{\partial}{\partial y}\left(D_i^{eff} \frac{\partial C_i}{\partial y} \right) \tag{12}$$

with

$$D_i^{eff} = \frac{C_i^{eq} D_i + \varepsilon_b C_b^{eq} D_b}{C_i^{eq} + \varepsilon_b C_b^{eq}} = D_i \frac{1 + \varepsilon_b s_i D_b / D_i}{1 + \varepsilon_b s_i}. \tag{13}$$

Here the segregation coefficient s_i is given by

$$s_i = \frac{C_b^{eq}}{C_i^{eq}}. \tag{14}$$

Note that the right-hand side of equation (13) coincides with equation (4) based on Hart's concept, which supports the validity of the present approach. Considering negligible diffusivity along GBs ($D_b \ll D_i$) in conjunction with strong segregation ($\varepsilon_b s_i > 1$) so that

$$\varepsilon_b s_i D_b / D_i \ll 1 \tag{15}$$

holds, equation (13) reduces to

$$D_i^{eff} = \frac{1}{1+\varepsilon_b s_i} D_i. \tag{16}$$

This effective diffusivity of any X atom reflects the fraction of diffusion time $1/(1+\varepsilon_b s_i)$ spent in the mobile (D_i-) configuration and a complementary time fraction spent in the virtually immobile ($D_b \approx 0$) X_b configuration. Since D_i^{eff} does not depend on local variables, it generates profiles of complementary error function type:

$$C_j = C_j^{eq} \operatorname{erfc}\left(\frac{y}{2\sqrt{D_i^{eff} t}}\right) \tag{17}$$

for X_i, X_b and therefore all X_j ($j = i, b, t$) provided that the diffusion source does not get exhausted. Notably, common radiotracer profiling techniques measure the total concentration C_t.

2.2.2. Regime γ: short diffusion times. As long as after the onset of the annealing treatment segregation does not play a significant role, diffusion times may be considered as effectively short. In this short-time regime, regime γ, equation (6*a*) and the reaction term of equation (6*b*) can be neglected. Impurity incorporation is then described to a good approximation by

$$\frac{\partial C_i}{\partial t} = D_i \frac{\partial^2 C_i}{\partial y^2} \tag{18}$$

inducing concentration–depth profiles of the form

$$C_i = C_i^{eq} \operatorname{erfc}\left(\frac{y}{2\sqrt{D_i t}}\right). \tag{19}$$

As will be shown below, the duration of the short-time period is connected with the reciprocal forward reaction rate k_{b+}.

2.2.3. Regime β: intermediate diffusion times. In this kinetic regime, segregation has begun to substantially affect the diffusion process but X_b and X_i have not yet attained a mutual state of local dynamical equilibrium. Hence, instead of equation (9) the inequality

$$C_b \ll \frac{C_b^{eq}}{C_i^{eq}} C_i \tag{20}$$

holds over almost the entire diffusion zone. Equation (20) implies, in conjunction with equations (7) and (8), that the reverse reaction terms in equations (6) may be neglected with respect to the forward terms, i.e.,

$$k_{b-} C_b C_{i0} \ll k_{b+} C_i C_{b0}. \tag{21}$$

Moreover, because of an approximate balance which establishes between X_i supply from the surface and X_i removal by segregation to GBs, the intermediate stage is subject to quasi-steady-state conditions; that is

$$\frac{\partial C_i}{\partial t} \approx 0. \tag{22}$$

The validity of this assumption has been confirmed by computer simulations [13, 14], namely, for pairs of diffusion–reaction equations conformable to equations (6*a*) and (6*b*). Inserting equations (21) and (22) into equation (6*b*) yields

$$\frac{\partial^2 C_i}{\partial y^2} = \frac{\nu_i}{D_i} C_i \tag{23}$$

where the transition frequency ν_i with dimension s^{-1} is given by

$$\nu_i = \varepsilon_b k_{b+} C_{b0} = \varepsilon_b s_i k_{b-} C_{i0}. \tag{24}$$

Here, the right-hand-side equality follows from equations (7) and (14). The solution of equation (23) for the pertinent boundary condition

$$C_i(y = 0, t) = C_i^{eq} \tag{25}$$

reads

$$C_i = C_i^{eq} \mathrm{e}^{-y/L_i} \tag{26}$$

where

$$L_i = \left(\frac{D_i}{\nu_i}\right)^{1/2} \tag{27}$$

may be conceived of as the mean free path of X_i atoms until they are captured by GBs. Neglecting again diffusion along GBs ($D_b \approx 0$) and utilizing equations (21) and (26), integration of equation (6*a*) leads to

$$C_b = k_{b+} C_{b0} C_i^{eq} t \mathrm{e}^{-y/L_i} \tag{28}$$

which complies with the appropriate initial condition

$$C_b(y, t = 0) = 0. \tag{29}$$

The total concentration as measured for instance in a radiotracer experiment leads with the aid of equations (10), (24), (25) and (27) to

$$C_t = (1 + \nu_i t) C_i^{eq} \mathrm{e}^{-y/L_i}. \tag{30}$$

2.2.4. Transient times. Now we will estimate the time limits within which the intermediate diffusion regime develops. For this purpose the maximum or total equilibrium concentration of X, C_t^{eq}, is written with the help of equations (10) and (14) as

$$C_t^{eq} = C_i^{eq} + \varepsilon_b C_b^{eq} = C_i^{eq}(1 + \varepsilon_b s_i) \tag{31}$$

and used together with equation (30) to normalize the actual C_t-values in the intermediate regime to

$$\frac{C_t}{C_t^{eq}} = \left(\frac{1 + \nu_i t}{1 + \varepsilon_b s_i}\right) \mathrm{e}^{-y/L_i}. \tag{32}$$

In order that the penetration profile be determined by segregation effects, $\varepsilon_b C_b$ must be much larger than C_i. In terms of equations (30) or (32) this means that $\nu_i t \gg 1$ must hold leading to the lower time limit

$$\tau_i^{\gamma\beta} = \nu_i^{-1} \tag{33}$$

separating the intermediate diffusion regime β from the short-time regime γ. The latter regime prevails if $\varepsilon_b C_b \ll C_i$ or $t \ll \tau_i^{\gamma\beta}$. On the other hand, to maintain the steady-state condition (22), X_b must stay far away from its saturation limit (cf. equation (21)). This is reflected by $C_t(0, t) \ll C_t^{eq}$ or

$$\frac{1 + \nu_i t}{1 + \varepsilon_b s_i} \ll 1 \tag{34}$$

imposing an upper time limit

$$\tau_i^{\beta\alpha} = \frac{\varepsilon_b s_i}{\nu_i} = \frac{1}{k_{b-} C_{i0}} \tag{35}$$

on the intermediate regime β. Within the present conditions of strong segregation ($\varepsilon_b s_i \gg 1$) it is easy to check that $\tau_i^{\beta\alpha} \gg \tau_i^{\gamma\beta}$. This implies that the time interval $\tau_i^{\gamma\beta} < t < \tau_i^{\beta\alpha}$ in which type-β diffusion evolves widens with increasing segregation (s_i) and GB volume (ε_b). When diffusion time exceeds $\tau_i^{\beta\alpha}$ the impurity incorporation process runs into regime α. The penetration profile thereby changes from an exponential-shaped to an erfc-like one as revealed by equations (30) and (17), respectively.

2.3. Interstitial–substitutional impurities

2.3.1. Basic concepts and equations. Experimental evidence for the occurrence of segregation-controlled diffusion emerged from the analysis of Au penetration profiles in Si. Here we have to account for the circumstance that the impurity is accommodated by the host lattice both interstitially (X_i) and substitutionally (X_s), the latter configuration being more abundant ($C_s^{eq} \gg C_i^{eq}$). Interchanges between these configurations may proceed either via the kick-out mechanism

$$X_i + S \underset{k_{I-}}{\overset{k_{I+}}{\leftrightarrow}} X_s + I \tag{36}$$

involving self-interstitials (I) or through the dissociative mechanism

$$X_i + V \underset{k_{V-}}{\overset{k_{V+}}{\leftrightarrow}} X_s + E \tag{37}$$

requiring the participation of vacancies (V). In equation (36) S denotes an occupied substitutional site of the host lattice.

A most general treatment would include, in addition to equations (6*a*) and (6*b*), three more diffusion–reaction equations, i.e., those for X_s, I and V. In practice, however, dislocations operate as sinks and sources for I and V. If the dislocation densities are high enough, the intrinsic point defects are kept at their thermal equilibrium concentrations; that is

$$C_I = C_I^{eq} \qquad C_V = C_V^{eq}. \tag{38}$$

According to the mass action relationships associated with reactions (36) and (37) which are similar to equations (7) and (8), one readily obtains by using equation (38)

$$C_s = \frac{C_i^{eq}}{C_s^{eq}} C_i. \tag{39}$$

The summation of the diffusion–reaction equation for X_s and equation (6*b*) for X_i yields

$$\frac{\partial C_l}{\partial t} = D_s \frac{\partial^2 C_s}{\partial y^2} + D_i \frac{\partial^2 C_i}{\partial y^2} - \varepsilon_b (k_{b+} C_i C_{b0} - k_{b-} C_b C_{i0}) \tag{40}$$

where the lattice concentration C_l of X is given by

$$C_l = C_i + C_s. \tag{41}$$

For interstitial–substitutional impurities, equation (40) replaces equation (6*b*) while equation (6*a*) remains valid. In equation (40) we ignore purely substitutional diffusion through X_s–V exchanges commonly known as the vacancy mechanism, i.e. $D_s \approx 0$, or more correctly $C_s^{eq} D_s \ll C_i^{eq} D_i$ [15, 16] (cf. equation (43)). Further, we introduce

$$\nu_{is} = \frac{C_i^{eq}}{C_i^{eq} + C_s^{eq}} \varepsilon_b k_{b+} C_{b0} = \frac{C_i^{eq}}{C_i^{eq} + C_s^{eq}} \nu_i \tag{42}$$

as the transition frequency of an average X atom in the lattice to an adjacent GB site,

$$D_{is} = \frac{C_i^{eq}}{C_i^{eq} + C_s^{eq}} D_i \tag{43}$$

as the effective diffusivity of such X atoms being alternately on interstitial and substitutional sites, and

$$s_{is} = \frac{C_b^{eq}}{C_l^{eq}} = \frac{C_i^{eq}}{C_i^{eq} + C_s^{eq}} s_i \tag{44}$$

as the proper GB segregation coefficient with regard to the total equilibrium concentration in the lattice $C_l^{eq} = C_i^{eq} + C_s^{eq}$. Using equations (39) and (41) to (44), it is straightforward to rearrange equations (6*a*) and (40) to

$$\frac{\partial C_b}{\partial t} = D_b \frac{\partial^2 C_b}{\partial y^2} + \frac{C_i^{eq} + C_s^{eq}}{C_i^{eq}} \frac{\nu_{is}}{\varepsilon_b} C_i - \frac{\nu_{is}}{\varepsilon_b s_{is}} C_b \tag{45a}$$

and

$$\frac{\partial C_i}{\partial t} = D_{is} \frac{\partial^2 C_i}{\partial y^2} - \left(\nu_{is} C_i - \frac{C_i^{eq}}{C_i^{eq} + C_s^{eq}} \frac{\nu_{is}}{s_{is}} C_b \right) \tag{45b}$$

respectively.

2.3.2. Kinetic regimes and diffusion profiles. The combined solution of equations (45*a*) and (45*b*) for interstitial–substitutional impurities produces similar kinetic regimes with similar diffusion profiles to that of equations (6*a*) and (6*b*) for purely interstitial impurities outlined in section 2.2. In particular, for diffusion times longer than

$$\tau_{is}^{\beta\alpha} = \frac{\varepsilon_b s_{is}}{\nu_{is}} \tag{46}$$

the X-incorporation process enters into regime α characterized by congruent erfc profiles of C_i, C_s and C_b and thus of the total concentration

$$C_t = C_i + C_s + \varepsilon_b C_b. \tag{47}$$

The effective diffusivity in regime α reads in analogy to equation (16)

$$D_{is}^{eff} = \frac{1}{1 + \varepsilon_b s_{is}} D_{is} \tag{48}$$

with D_{is} and s_{is} defined by equations (43) and (44). Obviously, this case is realized in the Si:Au experiment represented by figure 2.

For times distinctly shorter than

$$\tau_{is}^{\gamma\beta} = \frac{1}{\nu_{is}} = \tau_i^{\gamma\beta} \frac{C_i^{eq} + C_s^{eq}}{C_i^{eq}} \tag{49}$$

equations (45*a*) and (45*b*) predict a constant effective diffusivity D_{is} for both X_i and X_s which reflects in contrast to equation (48) the absence of segregation effects. Accordingly, the X distribution in this short-time regime, regime γ, evolves as

$$C_l = C_l^{eq} \operatorname{erfc}\left(\frac{y}{2\sqrt{D_{is} t}} \right). \tag{50}$$

For intermediate times $\tau_{is}^{\gamma\beta} \ll t \ll \tau_{is}^{\beta\alpha}$ the diffusion behaviour obeys regime-β kinetics described by

$$C_t = (1 + \nu_{is} t) C_l^{eq} \mathrm{e}^{-y/L_{is}} \tag{51}$$

with the characteristic diffusion length

$$L_{is} = \left(\frac{D_{is}}{\nu_{is}}\right)^{1/2}. \tag{52}$$

Experimental evidence for the occurrence of this type of behaviour is provided by figure 3.

3. Discussion

On the basis of equations (30) and (51) the mean square penetration $\langle y^2\rangle^\beta$ of impurity atoms in regime β is given by

$$\langle y^2\rangle^\beta = 2(L_k^\beta)^2 = 2D_k\nu_k^{-1} = 2D_k\tau_k^{\gamma\beta} \tag{53}$$

for $k = i, is$. The fact that $\langle y^2\rangle^\beta$ does not depend on diffusion time t complies with the quasi-steady-state conditions in this kinetic regime. Consistently with the Einstein–Smoluchowski relationship, $\tau_k^{\gamma\beta}$ has to be interpreted as the impurity mean time of residence in the lattice (characterized by diffusivity D_k) before being captured by a GB. Ignoring the unlikely situation that the transition from interstitial lattice sites to adjacent GB sites is considerably hampered by reaction barriers, $\tau_k^{\gamma\beta}$ reflects the average time needed to traverse a grain, i.e.,

$$\tau_k^{\gamma\beta} \approx \frac{G^2}{2D_k} \tag{54}$$

for $k = i, is$. Accordingly, L_k^β (or more precisely $\sqrt{2}L_k^\beta$) is intimately connected with the average grain size G. In terms of reaction-rate theory [17, 18] this means that k_{b+} is diffusion limited rather than reaction limited. Yet the impurity incorporation in regime β is significantly affected by the rate of segregation to grain boundaries and therefore may be conceived as being controlled by segregation or reaction. This is reflected by equations (27) and (30) or equations (51) and (52).

The above interconnection between L^β and G offers a clue to how to identify the present type of diffusion via experiments on polycrystalline material with known grain structure. We note that the L^β-values deduced from measured linear-type $\log C$ versus y profiles for diffusion of Au into Si (figure 3; see also [8, 12]) are compatible with the grain size of the sample materials employed. In general, however, L^β will also depend on grain structure (shape, size distribution, etc). This may be formally accounted for by including geometrical factors in the reaction constants entering equations (6*a*) and (6*b*). Such fine-tuning of the basic model is beyond the scope of the present first-order approach and therefore remains a future task. To some extent, the geometrical conditions are considered by taking $q = 2$ in equation (3).

Previous theoretical treatments of diffusion into polycrystalline matrices by Bokshstein *et al* [19] or Levine and MacCallum [20] explicitly take into account the special geometrical situation in polycrystals as compared to bicrystals. Although these treatments have their own merits, they naturally involve some approximations (like e.g. the assumption of spherical grains [19]), only apply to the case where (1) $D_b \gg D$, and moreover, are restricted to (2) low segregation levels and (3) equilibrium (detailed balance) between the diffusant in GBs and in the adjacent lattice (cf. [2]). By contrast, the present model deals with the essentially new situation where (1) $D_b \ll D$ and further makes allowance for (2) strong segregation, which in conjunction leads to (3) non-equilibrium between GB and lattice impurities. An extension of the standard models [19, 20] to the new conditions does not seem trivial and may form an attractive challenge for theoreticians in this field of research.

As a special feature, the present model includes blocking effects due to transversal grain boundaries characterized (like the other GBs) by $D_b \ll D$. Impurity atoms trapped by GBs become virtually immobile. At the bulk side of transversal boundaries these atoms may leak into deeper-lying grains in accordance with the reverse direction of equation (5). According to e.g. equations (20) and (21) this effect is not substantial until considerable accumulation of the impurity has taken place. Strong blocking at some lateral positions at a certain depth y are compensated by weak or negligible blocking conditions in other areas of the same depth layer. So, in terms of concentration averaged over xz-planes the physical situation is adequately reproduced by the quasi-continuum approach developed in the present paper.

Figure 1 gives a survey of the various kinetic regimes that may be encountered in impurity diffusion in polycrystalline materials. The upper half of this diagram compiles the profile shapes and key parameters characterizing the well known diffusion behaviour of types A, B and C for $D_b \gg D$ as outlined in the introduction. Transition times between the different regimes are also indicated [2, 4]. The lower half of figure 1 summarizes the stages of impurity incorporation derived under conditions of strong segregation and for $D_b \ll D$. Both interstitial and interstitial–substitutional impurities are comprised by the additional labelling of D, D^{eff}, L^{β} and s with the corresponding subscripts i or is, which is left to the reader.

It is remarkable that the two completely different physical situations under consideration ($D_b \gg D$ versus $D_b \ll D$) produce the same sequence of profile shapes, i.e., erfc, exponential-type, erfc. A distinction can only be made on the basis of quantitative analysis. As the most significant feature for $D_b \gg D$, impurity diffusion in polycrystals is enhanced with regard to that for single crystals of the same material. This may be recognized from the typical penetration lengths $L^C = (D_b t)^{1/2}$, L^B (see figure 1) and $L^A = (D^{eff} t)^{1/2}$ which exceed $(Dt)^{1/2}$ indicative of lattice diffusion. By contrast, for $D_b \ll D$ the pertaining penetration lengths $L^{\gamma} = (Dt)^{1/2}$, L^{β} (see figure 1) and $L^{\alpha} = (D^{eff} t)^{1/2}$ are smaller than or equal to $(Dt)^{1/2}$. Other criteria for discriminating between the two physical situations relate to the different nature of L^B and $L^{\beta} \approx G/\sqrt{2}$ and to dissimilar transition times, e.g., τ^{CB} in comparison with $\tau^{\gamma\beta}$ (see figure 1).

In fact, for interstitial–substitutional impurities the sequence of kinetic regimes has an extension (not shown in figure 1) towards lower diffusion times. This is connected with the establishment of local dynamic equilibrium between X_i and X_s as treated in the literature [13, 14]. Starting in regime γ and reducing diffusion time more and more we enter regime δ bounded by $\tau_{is}^{\varepsilon\delta} \ll t \ll \tau_{is}^{\delta\gamma}$ with

$$\tau_{is}^{\varepsilon\delta} = \frac{C_i^{eq}}{C_s^{eq}} \tau_{is}^{\delta y} = \frac{1}{k_{I+} C_{s0} + k_{V+} C_V^{eq}}. \tag{55}$$

Here k_{I+}, k_{V+} denote the X_i–X_s transition rates associated with reactions (36) and (37), respectively. Regime δ may be recognized from exponential-type profiles with the specific penetration depth $L^{\delta} = (D_i \tau_{is}^{\varepsilon\delta})^{1/2} < L^{\beta}$. For times even shorter than $\tau^{\varepsilon\delta}$ the transition from X_i to X_s has not started yet. In the corresponding regime, regime ε, diffusion proceeds purely interstitially, generating erfc profiles of typical depth $(D_i t)^{1/2}$ (cf. equation (19)).

Although the present paper does not aim at disclosing the physical reasons for the occurrence of segregation-controlled impurity diffusion, a few general comments seem appropriate. The type of diffusion under consideration is characterized by $\varepsilon_b s \gg 1$ and $\varepsilon_b s D_b \ll D$. Segregation to GBs appears to be inversely correlated with lattice solubility [21]. Thus, extremely high segregation coefficients s may be expected for a system like Si:Au which has a maximum solubility of 2×10^{17} cm^{-3} (attained about 100 K below the melting point T_m of pure Si) and solubilities in the ppb range or below at moderate

temperatures still accessible in diffusion experiments. Segregation can be further enhanced by the accompanying reduction of the GB energy [21]. An extreme example of GB saturation by impurities has been recently reported by Charaï and Rouvière [22] for S in Ge. It is conceivable that extremely high impurity concentrations in GBs lead to blocking effects with regard to atomic transport and thus to low D_b-values.

The circumstance that the diffusion behaviour treated here has been observed experimentally [8, 9, 12] for an interstitial–substitutional impurity (Au in Si [10]) gives rise to the following considerations. For impurities of this type, the lattice diffusivity D_{is} is given (under conditions of thermal equilibrium for vacancies and self-interstitials) by the interstitial diffusivity reduced by the factor $C_i^{eq}/(C_i^{eq} + C_s^{eq})$ representing the fraction of interstitial atoms (cf. equation (43)). Since D_i is large (10^{-4}–10^{-6} cm^2 s^{-1} in the high-temperature range) and $C_i^{eq}/(C_i^{eq} + C_s^{eq})$ not too small (10^{-1}–10^{-4}) an appreciable lattice diffusivity results which exceeds the estimated purely substitutional diffusivity through X_s–vacancy exchanges by orders of magnitude. It is further emphasized that the magnitude of the interstitial fraction depends sensitively on the atomic binding conditions in the interstices as well as on regular lattice sites.

Similarly, in GBs and their close vicinity one may distinguish between loosely bound impurity atoms with high mobility ($C_{b,m}$; $D_{b,m}$) and tightly bound atoms which are virtually immobile ($C_{b,im}$; $D_{b,im} \approx 0$). When it is tentatively assumed that the diffusivity $D_{b,m}$ of the mobile GB species compares to D_i, low effective GB diffusion coefficients may originate from mobile fractions $C_{b,m}/(C_{b,m} + C_{b,im})$ much smaller than $C_i^{eq}/(C_i^{eq} + C_s^{eq})$. In this way $D_b \ll D$ can be rationalized for interstitial–substitutional impurities.

4. Summary

Inspired by recent experimental observations regarding Au in Si, a new model has been proposed for impurity diffusion in polycrystalline materials. Specifically, the model applies to host material/impurity systems with the following properties:

(i) high diffusivity of the impurity through the lattice;
(ii) negligible diffusion along GBs; and
(iii) strong segregation to GBs which implies weak solubility in the lattice.

Experimentally, this particular combination of properties may be revealed by the following observations.

(1) The temporal evolution of the diffusion profile at constant temperature reveals a distinct sequence of shapes—erfc-like, exponential, erfc-like—characterizing the kinetic regimes γ, β and α, respectively.

(2) In the short-time regime, regime γ, the penetration depth is determined by the lattice diffusivity D of the impurity.

(3) In the intermediate regime, regime β, the mean penetration depth reflects the grain size G of the substrate.

(4) Transition from regime γ to regime β occurs after a diffusion time approximated by $G^2/2D$.

(5) After long diffusion times (regime α), penetration depth is reduced with respect to monocrystals of the same host material as well as compared to regime γ.

(6) GBs are enriched by impurities in regimes β and α.

Acknowledgment

One of us (NAS) thanks Dr Y Mishin for fruitful discussions and for making available several theoretical results prior to publication (see [2] and [4]).

References

[1] Kaur I, Gust W and Kozma L 1989 *Handbook of Grain and Interface Boundary Data* (Stuttgart: Ziegler)
[2] Kaur I, Mishin Yu and Gust W 1995 *Fundamentals of Grain and Interphase Boundary Diffusion* (Chichester: Wiley)
[3] Harrison L G 1961 *Trans. Faraday Soc.* **57** 1191
[4] Mishin Yu M and Herzig C 1995 *Nanostruct. Mater.* **6** 859
[5] Fisher J C 1951 *J. Appl. Phys.* **22** 74
[6] LeClaire A D 1963 *Br. J. Appl. Phys.* **14** 351
[7] Hart E W 1957 *Acta. Metall.* **5** 597
[8] Poisson C 1994 *Doctoral Thesis* Université Aix-Marseille III
[9] Poisson C, Rolland A, Stolwijk N A and Bernardini J 1993 *Diffusion and Defect Data A: Defect and Diffusion Forum* vols 95–98 (Switzerland: Trans. Tech.) p 393
[10] Stolwijk N A, Hölzl J, Frank W, Weber E R and Mehrer H 1986 *Appl. Phys.* A **39** 37
[11] Kühn B A 1991 *Doctoral Thesis* University of Stuttgart
[12] Poisson C, Rolland A, Stolwijk N A and Bernardini J 1996 *J. Appl. Phys.* submitted
[13] Bracht H, Stolwijk N A, Yonenaga I and Mehrer H 1993 *Phys. Status Solidi* a **137** 499
[14] Lever R F and Morehead F F 1993 *J. Appl. Phys.* **73** 1139
[15] Stolwijk N A 1990 *Phys. Status Solidi* b **157** 107
[16] Stolwijk N A 1993 *Diffusion and Defect Data A: Defect and Diffusion Forum* vols 95–98 (Switzerland: Trans. Tech.) p 895
[17] Atkins P W 1986 *Physical Chemistry* (Oxford: Oxford University Press)
[18] Waite T R 1957 *Phys. Rev.* **107** 463
[19] Bokshstein B S, Magidson I A and Svetlov I L 1958 *Phys. Met. Metallogr.* **6** 81
[20] Levine H S and MacCallum C J 1960 *J. Appl. Phys.* **31** 595
[21] Cabané J and Cabané F 1991 *Diffusion and Defect Data B: Solid State Phenomena* vols 15–16 (Switzerland: Trans. Tech.) p 1
[22] Charaï A and Rouvière J L 1994 *Mater. Res. Soc. Symp. Proc.* **319** 417